CHARACTERIZING ATMOSPHERIC TURBULENCE AND ITS IMPACT ON ELECTRO-OPTICAL SYSTEMS

OECD CONFERENCE CENTER, PARIS, FRANCE / 6 – 8 FEBRUARY 2018

Szymon Gładysz [(1)] and Karin Stein [(1)]

[(1)] Fraunhofer Institute of Optronics, System Technologies and Image Exploitation, Gutleuthausstr. 1, 76275 Ettlingen, Germany

KEYWORDS: atmospheric turbulence, adaptive optics, lasers

ABSTRACT:

Electro-optical (EO) systems, whether used for astronomical observations, remote-sensing and surveillance from space, tracking and high-resolution imaging of satellites, delivery of directed energy to space-based platforms, or horizontal-path imaging and laser communications, are always affected by atmospheric turbulence and in the majority of cases this turbulence imposes a fundamental limitation to their performance. In order to be able to compensate these effects one first needs to characterize turbulence: its strength and properties.

Most EO systems are operated in the lower atmospheric boundary layer which is highly affected by atmospheric turbulence. It is absolutely necessary to describe these optical disturbances in order to predict the performance of the systems.

Atmosphere is a complex system, so simplifications and approximations have to be made. We rely on statistical descriptions of turbulence to model its effect on EO systems. Kolmogorov's theory is the fundamental approach for the description of optical turbulence but it is not always valid, especially close to the ground where turbulence might not be fully developed and the short outer scale might seriously limit the range of spatial frequencies where Kolmogorov theory is valid, i.e. the inertial range.

To investigate the statistical behaviour of turbulence effects, Fraunhofer IOSB performed several experiments with a new technique based on differential motion measurements from an array of light-emitting diodes. The technique allows for measurement of not only the path-averaged turbulence strength but also of the outer scale, anisotropy coefficient, possibly non-Kolmogorov slope and transverse wind speed. The extracted values of these characteristics serve as input for simulations of laser beam propagation through realistic atmospheric turbulence.

1. INTRODUCTION

The local strength of optical turbulence is usually quantified through the refractive index structure parameter C_n^2 which relates to the relative strength of refractive index fluctuations separated by a unit distance. Given the value, or profile, of C_n^2 one can predict the values of focal plane observables such as beam or image motion, scintillation index, beam spreading, etc. It is therefore a parameter of fundamental importance for the design of EO systems operating within the Earth's atmosphere.

Path-integrated C_n^2 can be measured with a scintillometer. This measurement yields estimates which are mostly influenced by turbulence in the middle of the path. Strong turbulence there would bias the result. On the other hand, the angle-of-arrival method, based on the measurement of absolute image motion, is more sensitive to turbulence close to the sensor. Neither of these methods has the flexibility allowing one to adjust the measurement sensitivity to a certain location along the path. This is one of the reasons why we developed an approach which permits choosing this sensitivity/weighting function (see Figure 1).

The angle-of-arrival approach is susceptible to transmitter's and receiver's vibrations, drifts, thermal effects on optics, etc. Measurement of *differential* image motion is not affected by any of these effects. Additionally, with an array of transmitters (here light-emitting diodes – LEDs) one can obtain a high-SNR estimate of C_n^2. Although Shack-Hartmann sensor will see more motion in each lenslet, an LED array will give a 100-times better SNR per measurement. This means that an LED array will still work when Shack-Hartmann will yield only noise. Additionally, sampling of the tilt structure function can be much better controlled with an array of transmitters because one has complete freedom where to position the sources and in which geometry. Another advantage of observing with a full aperture is reduction of image scintillation due to aperture averaging. Finally, it is worth noting that fabrication of an LED array is significantly cheaper than manufacturing of a lenslet array.

In this paper the methodology of extracting not only path-integrated C_n^2 but also other parameters of interest such as e.g. outer scale or non-Kolmogorov spectral slope from video sequences of an LED array will be outlined. Some results from a field trial at the proving ground belonging to Institute of Saint-Louis (ISL) in Baldersheim, France, will be shown.

2. METHODOLOGY

Differential motion, i.e. tip or tilt, in the direction parallel ($\sigma_\parallel^2$) or perpendicular ($\sigma_\perp^2$) to the sources' separation *d* is a structure function:

$$\sigma_{\parallel,\perp}^2 \equiv D_\theta(d) \equiv \langle \big(\theta(r) - \theta(r+d)\big)^2 \rangle \qquad (1)$$

where θ is the angle of arrival (tip/tilt), *D* denotes structure function, and $\langle . \rangle$ denotes ensemble average. The theoretical expression giving the magnitude of differential motion is derived by filtering the two-dimensional Kolmogorov spectrum of phase and including the anisoplanatic term. Filtering is done either with the gradient-tilt ("G-tilt") or the Zernike-tilt ("Z-tilt") filter functions [1]. For the two components, *x* and *y*, of G-tilt we have

$$\begin{bmatrix} F_{x,G}(\boldsymbol{\kappa}) \\ F_{y,G}(\boldsymbol{\kappa}) \end{bmatrix} = \left(\frac{4}{k_0 D}\right)^2 J_1^2(\gamma\kappa D/2) \begin{bmatrix} \cos^2(\varphi) \\ \sin^2(\varphi) \end{bmatrix} \qquad (2)$$

where $\boldsymbol{\kappa}$ is the 2-D spatial frequency (of magnitude κ and angle φ), $k_0 \equiv \frac{2\pi}{\lambda}$ is the wavenumber, γ is the propagation parameter (z/*L* for spherical wave, where *z* is the coordinate along the propagation path and *L* is the total propagation distance), and $J_n(.)$ is Bessel function of order *n*. From now on *D* will denote the diameter of the entrance pupil of the sensor unless the structure function is explicitly mentioned. For Z-tilt the expressions are

$$\begin{bmatrix} F_{x,Z}(\boldsymbol{\kappa}) \\ F_{y,Z}(\boldsymbol{\kappa}) \end{bmatrix} = \left(\frac{16}{k_0 D}\right)^2 \left[\frac{J_2\left(\frac{\gamma\kappa D}{2}\right)}{\frac{\gamma\kappa D}{2}}\right]^2 \begin{bmatrix} \cos^2(\varphi) \\ \sin^2(\varphi) \end{bmatrix} \qquad (3)$$

It is important to determine which tilt, G-tilt or Z-tilt, a given motion estimator actually measures. Some estimators, e.g. centroid or correlation, yield results compatible with G-tilt while other estimators might follow Z-tilt [2]. We give here expressions for differential motion in the case of G-tilt:

$$\begin{bmatrix} \sigma_\parallel^2 \\ \sigma_\perp^2 \end{bmatrix} = 0.2073 \int_0^L dz\, C_n^2(z) \int d\boldsymbol{\kappa} \begin{bmatrix} \cos^2(\varphi) \\ \sin^2(\varphi) \end{bmatrix} \kappa^{-\frac{11}{3}} \left(\frac{4}{D}\right)^2 \times J_1^2\left(\frac{z\kappa D}{2L}\right) 2\left\{1 - \cos\left[\kappa d \frac{L-z}{L}\cos(\varphi)\right]\right\} \qquad (4)$$

where we have explicitly included the spherical-wave propagation factor *z*/*L* and Kolmogorov turbulence model was assumed. After some simplifications [3] one can arrive at the result

$$\begin{bmatrix} \sigma_\parallel^2 \\ \sigma_\perp^2 \end{bmatrix} = \frac{41.7}{D^2} \int_0^L dz\; C_n^2(z) \begin{bmatrix} I_T - I_1 \\ I_1 \end{bmatrix} \qquad (5)$$

with

$$I_1 = \int_0^\infty d\kappa\, \kappa^{-8/3} J_1^2\left(\frac{z\kappa D}{2L}\right)\left(\frac{1}{2} - \frac{J_1[\kappa d(L-z)/L]}{\kappa d(L-z)/L}\right)$$

$$I_T = \int_0^\infty d\kappa\, \kappa^{-8/3} J_1^2\left(\frac{z\kappa D}{2L}\right)(1 - J_0[\kappa d(L-z)/L])$$

Similar analysis must be performed for Z-tilt anisoplanatism using filter function from Equation (3).

Reader's attention is directed to the $(L-z)/L$ term in Eqs. (4) and (5). This term is missing in Refs. [1] and [3]. While the physical separation between the sources in the object plane, *d*, is constant, it is the separation between the *waves* which induces anisoplanatism and this separation depends on *z*. In the pupil plane the separation between the waves is zero (there is no anisoplanatism). It is well known that a thin layer of turbulence in front of the pupil is fully isoplanatic.

It is instructive to compute the C_n^2 weighting function from Eq. (5) [4]. When this equation is cast in the form $\sigma_{\parallel,\perp}^2 = \int_0^L dz\; C_n^2(z) f_{\parallel,\perp}(z)$, then the path weighting function $f_{\parallel,\perp}(z)$ changes dramatically depending whether one includes the $(L-z)/L$ term in Eqs. (4) and (5) or not. The differences are illustrated in Figure 1. This can lead to discrepancies with other measurement methods [5]. The error is a factor of around 3 underestimate of C_n^2.

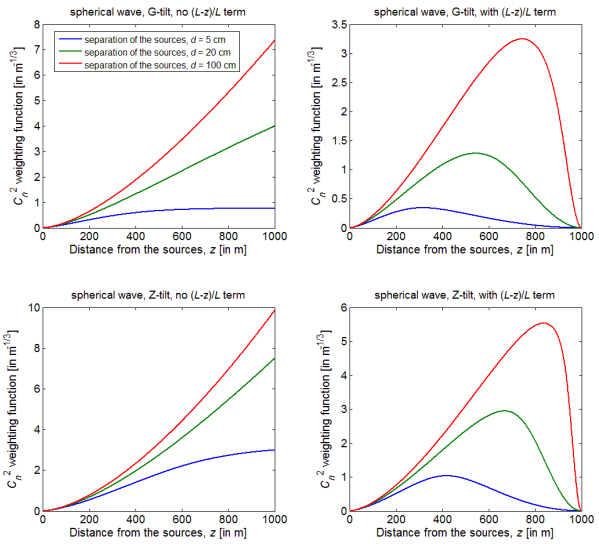

Figure 1. Tilt anisoplanatism path-weighting functions $f_{\parallel,\perp}(z)$ for various propagation scenarios and theoretical models, L = 1 km, D = 10 cm, which are typical values in our long-range experiments. Top: G-tilt. Bottom: Z-tilt. Left: no $(L-z)/L$ term. Right: with $(L-z)/L$ term.

An LED array offers a very simple way to measure outer scale, L_0, independently from C_n^2. First, re-write Equation (4) for the von Kármán model, assuming constant C_n^2 along the path:

$$\begin{bmatrix}\sigma_{\parallel}^2\\ \sigma_{\perp}^2\end{bmatrix} = \frac{6.6336\, C_n^2}{D^2}\int_0^L dz \int d\boldsymbol{\kappa} \begin{bmatrix}\cos^2(\varphi)\\ \sin^2(\varphi)\end{bmatrix} (\kappa^2+\kappa_0^2)^{-\frac{11}{6}} \times J_1^2\left(\frac{z\kappa D}{2L}\right)\left\{1-\cos\left[\kappa d\,\frac{L-z}{L}\cos(\varphi)\right]\right\} \quad (6)$$

where $\kappa_0 = \frac{2\pi}{L_0}$. Note that parallel and perpendicular variances have different functional forms and that C_n^2 is outside the integral. The ratio of $\sigma_{\parallel}^2$ and $\sigma_{\perp}^2$ cancels out the C_n^2 dependence and has only one unknown, that is L_0. Non-Kolmogorov power spectrum exponent can be estimated in a similar fashion [3]. Level of anisotropy can be measured by comparing C_n^2 and L_0 values in the horizontal and vertical directions.

Transverse wind speed can be measured by re-writing the equations above in the temporal domain. First, construct the spatio-temporal structure function of motion:

$$D_\theta(d,\tau) = \langle[(\theta(r,t)-\theta(r+d,t)) -(\theta(r,t+\tau)-\theta(r+d,t+\tau))]^2\rangle \quad (7)$$

where τ is the temporal lag between two samples. This form of the spatio-temporal structure function is again independent of any sources of global image motion. In order to make use of the known relationships derived in the spatial domain we adopt the Taylor hypothesis which states that the phase is translated at the wind velocity *V*, its shape remaining unchanged (frozen turbulence approximation). Tilt being directly related to the phase, the assumption applies to θ as well, and one can write

$$\theta(\mathbf{r}, t+\tau) = \theta(\mathbf{r}-\tau\mathbf{V}, t) \quad (8)$$

After some manipulations one arrives at the result which depends only on spatial-domain quantities:

$$D_\theta(d,\tau) = 2D_\theta(d,0) + 2C_\theta(d-\tau\boldsymbol{V},0) +2C_\theta(d+\tau\boldsymbol{V},0) - 4C_\theta(\tau\boldsymbol{V},0) \quad (9)$$

In Equation (9) $D_\theta(d,0)$ is the purely spatial structure function of tilt given by Eqs. (4) and (5), $C_\theta(d,0)$ is the purely spatial auto-covariance of motion which can be derived in a similar fashion as Eqs. (4) and (5). When implementing Equation (9) for spherical waves, as is the case here, it is important to take into consideration the so-called apparent wind [6]. With the assumption of uniform wind velocity along the propagation path this means replacing *V* in the equations above with *VL*/*z*.

Equation (9) is very useful because it fully describes, both in the spatial as well as in the temporal domain, turbulence-induced image motion, and additionally it does so in a way that neglects all possible artificial sources of motion. In Figure 2 the spatio-temporal structure function of motion is plotted for typical parameters of the atmospheric turbulence.

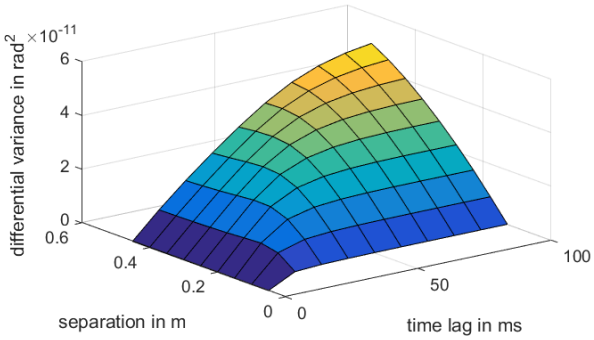

Figure 2. Spatio-temporal structure function of motion for a typical scenario of propagation in air, L = 300 m, D = 25 cm, $C_n^2 = 10^{-14}m^{-2/3}$, and V = 4 m/s, which are the values we set, or expect, in our most recent short-range experiments.

Estimation of *V* from experimental data is done by computing several templates of Equation (9) for various plausible flow velocities and then checking which template fits experimental spatio-temporal differential variances the best, in the least-squares sense.

3. EXPERIMENT

Over two days, 28th and 29th of July 2015, we performed experiments on the proving ground of French-German Research Institute of Saint-Louis in Baldersheim, France. Both days were quite hot, with temperatures near 30°C around midday. Our array consists of 10×10 white-light LEDs separated by 5 cm. It was positioned 270 m from the receiver, a 145-mm diameter lens coupled with the 4.2MP CMOS sensor (RAPTOR Osprey, 12-bit, 5.5µm pixels, TE-cooled) running at 100 Hz in subarray mode. Both devices were positioned around 1 m above the ground. Thousand 1-ms long frames were stored every two minutes.

As reference for the results from the LED array, a scintillometer (BLS 900 from Scintec) and a PSF/MTF-based measurement setup were also employed during the trial. The latter setup was developed at Fraunhofer IOSB as a portable means of estimating turbulence strength from Fried's "short-exposure" modulation transfer function (MTF) [7]. As can be seen in Figure 3 there is a good agreement between the methods. As expected, outer scale is quite short, on average around 60 cm (Figure 4).

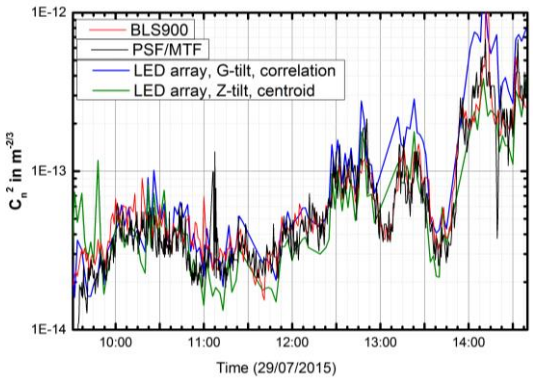

Figure 3. Comparison of results of the four C_n^2 measurement methods from three devices.

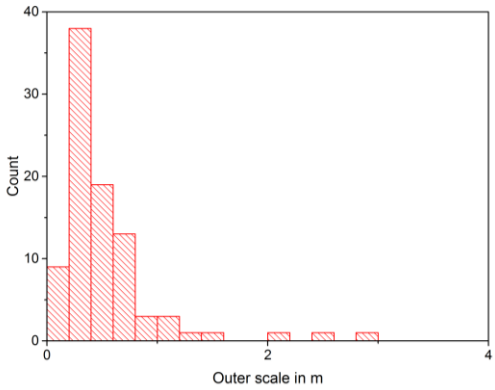

Figure 4. Histogram of outer scale measurements.

4. RELEVANCE TO LASER BEAM PROPAGATION THROUGH THE ATMOSPHERE

In this section we will show that the knowledge of only path-averaged refractive index structure parameter C_n^2 is not sufficient to accurately predict the shape of the Gaussian beam spot in the receiver or target plane. We will do so on the example of the effect of finite outer scale as opposed to the assumption of the infinite outer scale made implicitly in the Kolmogorov model.

Monte-Carlo simulations have been carried out for the scenario of a focused Gaussian beam propagation through 1 km of atmospheric turbulence with a constant C_n^2. The other parameters of these particular simulations are restricted.

Figure 5 shows in the top row the beam spot images for the Kolmogorov turbulence model, for three turbulence strengths: C_n^2 = 0 (no turbulence; propagation in vacuum), C_n^2 = 10^{-15} $m^{-2/3}$ and C_n^2 = 10^{-14} $m^{-2/3}$. The bottom row shows corresponding beam images for the same turbulence strengths but with a more realistic outer scale value of 1 m, for propagation close to the ground. It is clear that when turbulence gets stronger the impact of finite outer scale becomes very clear. Outer scale is responsible for the suppression of low-order aberrations acting on the beam. The most important effect is the reduction of beam wander.

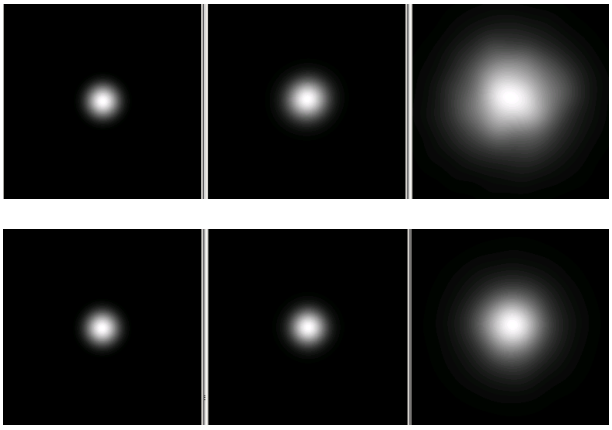

Figure 5. Top row: averaged results of Monte-Carlo simulations for laser beam propagation through pure Kolmogorov turbulence ($L_0 = \infty$). From left to right: propagation in vacuum, $C_n^2 = 10^{-15}$ $m^{-2/3}$ and $C_n^2 = 10^{-14}$ $m^{-2/3}$. Bottom row: simulations corresponding to more realistic value of outer scale: L_0 = 1 m. Each picture corresponds to an average of 5000 uncorrelated realizations.

5. CONCLUSIONS

In this paper a method for extraction of several parameters of optical turbulence based on differential image motion was presented. Sample results for path-averaged refractive index structure constant and the outer scale were presented. With this paper we tried to convince the reader of the importance of *full* characterization of optical turbulence for the task of EO system design. The performance of correction methods such as adaptive optics, in particular, is highly dependent on the profile of C_n^2 along the path, on the value of the outer scale which will determine the necessary deflection of the tip/tilt mirror, and on the transverse wind velocity which will determine the required loop rates of the system.

6. ACKNOWLEDGMENTS

This research is part of the project LIMIS-UM, E/E91S/GC025/GF010, commissioned and sponsored by the WTD91 (Technical Centre of Weapons and Ammunition) of the German Armed Forces.

7. REFERENCES

[1] R. J. Sasiela, Electromagnetic wave propagation in turbulence. Evaluation and application of Mellin transforms, 2nd ed. (SPIE, 2007).

[2] D. A. LeMaster, R. C. Hardie, S. Gladysz, M. D. Howard, M. A. Rucci, M. E. Trippel, J. D. Power, B. K. Karch, "Differential tilt variance

effects of turbulence in imagery: comparing simulation with theory," Proc. SPIE 9846, (2016).

[3] S. Gladysz, M. Segel, C. Eisele, R. Barros, E. Sucher, "Estimation of turbulence strength, anisotropy, outer scale and spectral slope from an LED array," Proc. SPIE 9614, (2015).

[4] R. C. Hardie, J. D. Power, D. A. LeMaster, D. R. Droege, S. Gladysz, S. Bose-Pillai, "Simulation of anisoplanatic imaging through optical turbulence using numerical wave propagation with new validation analysis," Opt. Eng. 56(7), 071502 (2017).

[5] R. Forsling, "Time constants of optical turbulence in the atmosphere," MSc thesis, Umeå University, (2016).

[6] J.-M. Conan, G. Rousset, and P.-Y. Madec, "Wave-front temporal spectra in high-resolution imaging through turbulence," J. Opt. Soc. Am. A 12, 1559-1570 (1995).

[7] Yatcheva, L., Barros, R., Segel, M., Sprung, D., Sucher, E., Eisele, C., and Gladysz, S., "Ultimate turbulence experiment: simultaneous measurements of Cn2 near the ground using six devices and eight methods," Proc. SPIE 9641, (2015).